Nanocomposite fabrics with high content of boron nitride nanotubes for tough and multifunctional composites

Martinez-Rubi, Yadienka; Ashrafi, Behnam; Jakubinek, Michael B.; Zou, Shan; Kim, Keun Su; Cho, Hyunjin; Simard, Benoit

Publisher's version / Version de l'éditeur:
https://doi.org/10.1557/s43578-022-00707-x
Journal of Materials Research, 37, 24, pp. 4553-4565, 2022-12-28

Journal of MATERIALS RESEARCH

Article
DOI:10.1557/s43578-022-00707-x

BORON NITRIDE NANOTUBES

FOCUS ISSUE

Nanocomposite fabrics with high content of boron nitride nanotubes for tough and multifunctional composites

Yadienka Martinez-Rubi[1,a], Behnam Ashrafi[2], Michael B. Jakubinek[1], Shan Zou[3], Keun Su Kim[1], Hyunjin Cho[1], Benoit Simard[1]

[1] Security and Disruptive Technologies Research Centre, National Research Council Canada, Ottawa, ON, Canada
[2] Aerospace Research Centre, National Research Council Canada, Montreal, QC, Canada
[3] Metrology Research Centre, National Research Council Canada, Ottawa, ON, Canada
[a] Address all correspondence to this author. e-mail: Yadienka.martinez-rubi@nrc-cnrc.gc.ca

Received: 14 April 2022; accepted: 15 August 2022; published online: 7 September 2022

Michael Jakubinek was a guest editor of this journal during the review and decision stage. For the JMR policy on review and publication of manuscripts authored by editors, please refer to http://www.mrs.org/editor-manuscripts/

Herein, we apply a one-step filtration method to obtain boron nitride nanotube (BNNT)-based fabrics incorporating high content of BNNTs and an adhesive thermoplastic polyurethane (TPU). The adsorption behavior of TPU on BNNTs of different qualities and on functionalized BNNTs was evaluated in a two-solvent system and contrasted with carbon nanotubes, pointing to differences in surface interaction. BNNT quality affected not only the nanocomposite mechanical properties but also the trends as a function of increasing TPU content and the adhesion to substrates. Samples containing higher quality BNNT materials showed up to 12-fold improvement in Young's modulus, while functionalization improved the tensile toughness. Thermal conductivity varied between 1.5 and 3 W m^{-1} K^{-1} depending primarily on the BNNT content and without a pronounced effect from the quality of BNNTs. The BNNT-TPU fabric offers a promising format to exploit BNNTs within tough, electrically insulating, thermally conductive materials for heat dissipation within packaging or adhesive materials in electronics.

Introduction

The development of low-dimensional boron nitride (BN) materials, such as boron nitride nanotubes (BNNTs), parallels that of their carbon equivalents (carbon nanotubes, graphene, etc.). Research in this area has increased in recent years due to new synthetic methods and increased availability of the materials such as BNNTs [1]. BNNTs are structural analogues to carbon nanotubes (CNTs) and possess similar mechanical properties with reported values of Young's modulus as high as ~ 1 TPa and maximum stress of ~ 60 GPa [2]. However, the polarity of the BN bond imparts partial ionic characteristic of BN materials, which leads to different and complementary functional properties compared to nano-carbon materials. BNNTs are wide bandgap semiconducting materials with a nearly constant bandgap (~ 6.0 eV) regardless of chirality, diameter, or the number of walls [3]. They are transparent in the visible region of the electromagnetic spectrum, exhibit electrical insulation with high thermal conductivity (350 W m^{-1} K^{-1}) [4], and have higher thermo-oxidative stability than CNTs [5]. Due to the presence of boron, BNNTs are also effective absorbers for neutron radiation [6]. All these characteristics have attracted research interest for different applications of BNNTs and other BN structures [7–10]. Partially due to their highly polarized electrical characteristics and the resulting strong Coulomb interactions, BNNTs are capable of forming strong binding interfaces with polymer matrices such as epoxies showing a superior interfacial load transfer capacity in composites relative to CNTs [11]. Fiber-reinforced polymer composites incorporating BNNTs into the epoxy matrix showed enhancements in shear and impact properties of the hybrid composites [12] while incorporation into an epoxy adhesive also led to increased lap shear strength associated with observations of pull-out of BNNTs at the failure surfaces [13].

Recently electrically insulating yet thermal conductive polymer composites have been widely explored for application in thermal management of electronics, and in these applications, high BN loadings are usually required while achieving simultaneous high ductility [14, 15]. In the case of BNNTs, polymer composites with high BNNT content (~25–35 wt%) have been reported to have thermal conductivities of 1.5–4 W m^{-1} K^{-1} [16, 17], which is in the range of 5 to 25 times higher than the polymer matrix. Other potential applications of polymer composites with high BN content have been reported, including thermally conductive flexible adhesives [18] and neutron radiation shielding [19].

Development of non-woven sheets or fabrics offers a practical route to achieve high reinforcement content in nanocomposites, which is often required to realize the desired multifunctional properties for a particular application. Lightweight nanotube buckypapers and nanotube/polymer composite sheets with high nanotube content are also attractive because they simplify the handling of nanomaterial and can be readily integrated into conventional composite systems as well as laminated structures [20–24]. We recently developed a one-step filtration method for the fabrication of such nanocomposite fabrics using CNTs and a thermoplastic polyurethane adhesive (TPU) [22, 25]. The method uses a TPU solvent/non-solvent combination to enhance polymer interaction with nanotubes and to facilitate a fast recovery of non-woven nanocomposite sheets of controlled and tailorable composition by vacuum filtration. We demonstrated that the adsorption of TPU on CNTs can be controlled through solubility modulation and TPU chains mainly form a stable shell or coating around the CNTs leaving a low concentration of TPU in solution. CNT-TPU nanocomposites can then be recovered by vacuum filtration in a very short time as a non-woven sheet made of highly entangled and randomly oriented CNT/TPU "nano-fibers." The network packing and possibly the nanotubes exfoliation were also shown to depend on the nanotube to TPU ratio. This new method of producing nanocomposite sheets is in contrast to processing methods that involve the fabrication of a high nanotube content preform or buckypaper followed by a polymer infiltration step [21, 26].

Here, we report the development of BNNT-TPU nanocomposite sheets of variable composition via the one-step vacuum filtration process applied to BNNT materials with different quality. Adsorption of TPU on pristine and non-covalently functionalized BNNTs, respectively, was studied and compared to the behavior observed with CNTs. The observed different interactions between TPU and BNNTs, in comparison with CNTs, correlate to the differences in tensile mechanical properties. Elastic modulus mapping by atomic force microscopy (AFM) was employed to analyze the complex morphology of the nanocomposite sheets revealing significantly different mechanical responses depending on the nanotube type. The resulting tough and thermally conductive BNNT composites are promising for heat dissipation within packaging or adhesive materials in electronics, and potentially for other applications such as neutron shielding of space structures that would also benefit from robust polymer composites with added multifunctional features of BNNTs.

Results and discussion

Different TPU adsorption behavior on BNNTs

BNNT-TPU sheets of variable composition were fabricated by applying a one-step filtration process previously reported for CNT-TPU composite sheets [25]. The method is based on the controlled adsorption of TPU on high surface area nanotubes (~250 m^2/g for CNTs) dispersed in a TPU solvent/non-solvent mixture. At an optimized solvent/non-solvent ratio, by simply changing the concentration of TPU in solution (increasing the TPU:CNT ratio), it is possible to readily recover nanocomposite sheets with controlled composition and tailorable properties. Using this approach, in the presence of CNTs, upon mixing with the non-solvent, a significant fraction of the dissolved TPU (~70%) is separated from the solution and immobilized onto the surface of the CNTs rather than coagulated in the solvent mixture facilitating the fast recovery of non-woven sheets by vacuum filtration. The conditions and solvent/non-solvent ratios previously employed for the fabrication of CNT-TPU sheets were initially applied to the BNNT-TPU system (see Supplementary Information). Under those conditions, contrary to the case of CNTs, coagulation of the TPU rather than immobilization onto the surface of the BNNTs as result of non-covalent van der Waals interactions was still evident (Fig. S1). This made the recovery of the sheets difficult by filtration due to a high concentration of polymers blocking the membrane filter. The BNNT-1 and BNNT-2 materials employed in this study were obtained from two different purification batches producing materials with specific surface areas of 180 m^2/g and 250 m^2/g, respectively, with the latter being comparable to the specific surface area of CNT previously employed. The BNNT material was also evaluated using the recently developed method for quality assessment (see Fig. S2), which also indicated higher quality of the BNNT-2 material compared to BNNT-1 in agreement with SEM imaging results (Fig. S3). In the presence of both BNNT materials, regardless of the surface area and quality, coagulation of the free polymer was observed rather than immobilization of the polymer onto the surface of the BNNTs. This clearly confirmed a weaker interaction of the TPU with BNNTs in comparison with CNTs. Nevertheless, by increasing the concentration of BNNTs and the non-solvent to solvent ratio, it was possible to force the adsorption of TPU onto the BNNT surface, allowing the recovery of nanocomposite sheets by vacuum filtration.

Table 1 summarizes the compositional properties of BNNT-TPU nanocomposite sheets with different BNNT/TPU weight

ratios obtained by changing the BNNT:TPU ratio in the solvent mixture (*i.e.*, BNNT:TPU weight ratios of 1:1, 1:1.5, 1:2, 1:3, and 1:4 in solution). Note that in all cases, the amount of TPU adsorbed on the nanotubes, and that appears in the composite fabric recovered after filtration, is lower than the initial amount added in solution, as determined by the partition coefficient of TPU on nanotube to the concentration of TPU in the liquid phase [25]. The lowest BNNT (highest TPU) content that is possible to attain using this method is limited by the increased adhesion of the nanocomposites to the PTFE filter membrane as the TPU content increases, which prevents detachment and the complete recovery of the dried nanocomposite sheets. It was observed that this limit of BNNT/TPU composition varied depending on the quality of the BNNT material used (*e.g.*, 31/69 and 26/74 for BNNT-1 and BNNT-2, respectively, in Table 1).

The densities of the BNNT-TPU sheets indicate that all the nanocomposites are porous in nature. Although not as clear as for the case of CNT-TPU sheets, where an optimal network packing was evident at a CNT/TPU composition of 35/65 by weight [25], measurements of the sheets thickness and calculations of the void fraction (Table 1) are also indicative of a network densification at a critical BNNT/TPU weight ratio. For example, for BN2-PU sheets (with higher purity BNNTs), the volume faction of BNNTs (vol%) is relatively constant for BN2-PU-1, BN2-PU-1.5, and BN2-PU-2 as the TPU content increases, while the sheet thickness and void content show minimum values for BN2-PU-2 sheets (BNNT/TPU composition of 42/58 by weight). Although the void fraction decreases as the TPU content increases, as expected, it increases at BNNT vol% lower than 23% for BNNT-1 and 19% for BNNT-2 nanocomposites. This increase in the void fraction is indicative of a deterioration of the network packing. Table 1 also includes sheets fabricated using functionalized BNNTs (f-BNNT-2). In this case, the BNNTs were noncovalently functionalized with regiorandom poly(3-hexyl-thiophene) (rra-P3HT) prior to integration with TPU. The conjugated rra-P3HT polymers self-assemble on BNNTs via π-π stacking [27], producing a stable and uniform dispersion of exfoliated rra-P3HT/BNNT hybrids in $CHCl_3$ and could potentially influence the interactions at the BNNT-TPU interface. The presence of hydrophobic alkyl chains on the BNNT surface could result in a favorable interaction with the hydrophobic segments of TPU.

The adsorption behavior, defined as the process through which a net accumulation of a substance occurs at the common boundary of two contiguous phases, was evaluated for BNNTs. Similar studies were previously undertaken to describe surface modification of CNTs with TPU in the production of CNT-TPU nanocomposites [25]. The degree of TPU adsorption (C_{ads}) by BNNTs was determined using the mass balance (Eq. 1). Using this procedure, however, it can be difficult to discriminate between real adsorption and phase separation, especially considering the observed lower affinity of TPU to BNNT. The complex behavior is described in Fig. 1 by plotting the solute (*i.e.*, TPU) concentration in the liquid phase (C_{eq}) on the *x* axis versus C_{ads} on the *y* axis. It can be observed that the adsorption behavior of TPU to BNNT-1 and BNNT-2 was similar, while functionalized

TABLE 1: Physical properties of the BNNT-TPU sheets recovered by the one-step filtration method by changing the BNNT:TPU ratio in the solvent mixture (See "Methods" section).

	BNNT-TPU sheets recovered by vacuum filtration					
				Volume fraction (vol%)		
Sample name[a]	BNNT/TPU weight ratio (w/w)	Density (g/cm^3)	Thickness (μm)	BNNT	TPU	Void
BN1-PU-1	60/40	0.93	56	29	31	40
BN1-PU-1.5	49/51	1.00	63	26	42	32
BN1-PU-2	42/58	1.06	71	23	51	25
BN1-PU-3	31/69	0.97	104	16	56	28
BN2-PU-1	60/40	0.77	68	25	25	50
BN2-PU-1.5	49/51	0.91	70	23	39	38
BN2-PU-2	42/58	1.14	66	25	56	19
BN2-PU-3	31/69	1.19	85	19	69	11
BN2-PU-4	26/74	0.99	123	14	61	25
f-BN2-PU-1	54/46	0.81	72	23	31	46
f-BN2-PU-1.5	44/55	0.88	80	21	41	38
f-BN2-PU-2	39/61	1.15	71	23	59	18
f-BN2-PU-3	29/71	1.19	91	18	71	11
f-BN2-PU-4	23/77	1.11	123	14	71	15

[a]Note that in the sample labels (BNx-PU-y), *x* indicates the type of BNNTs (*e.g.*, BNNT-1 or BNNT-2) and *y* indicates the TPU to BNNT weight ratio in the solvent mixture, before filtration, while *f* corresponds to functionalized BNNTs with rra-P3HT.

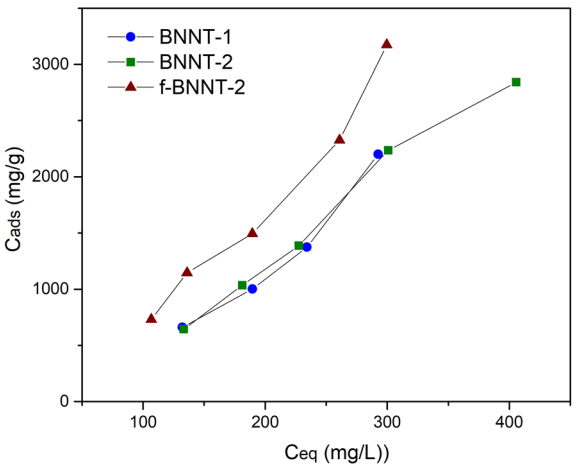

Figure 1: Adsorption data of TPU on BNNTs in the solvent/non-solvent mixture for BNNT-1 (blue filled circle), BNNT-2 (green filled square) and f-BNNT-2 (brown filled triangle).

BNNTs (f-BNNT-2) show higher adsorption (*i.e.*, higher C_{ads} for a given C_{eq}). This is attributed to an improved interaction between TPU and the modified BNNTs with rra-P3HT (which allows BNNT to be more exfoliated), leading to the recovery of higher TPU content sheets and reduced void fraction (*e.g.*, 25 void% vs. 15 void% for BN2-PU-4 and f-BN2-PU-4, respectively, in Table 1) at equivalent fabrication conditions. It is worth mentioning that, in contrast to the observations with BNNTs, similar sheets incorporating h-BN, instead of BNNTs, cannot be produced using this one-step filtration method due to a weak interaction with TPU and inefficient h-BN exfoliation (low specific surface area). In the presence of h-BN, TPU adsorption was not favored and composite sheets cannot be readily recovered by vacuum filtration.

Figure 2 shows representative SEM images of the surface of BNNT-TPU composite sheets fabricated by the one-step filtration method at different TPU contents incorporating BNNT-1 and BNNT-2 materials. SEM images of the purified BNNTs employed in this study are shown in Fig. S3. Figures 2 and S3 show that both BNNT materials still contain BN impurities (non-tubular features), although a higher content of impurity can be observed in the BNNT-1 material, in agreement with the quality assessment results (Fig. S2). Similar to the previous observations for CNT-TPU sheets (Fig. S4), the BNNT-TPU

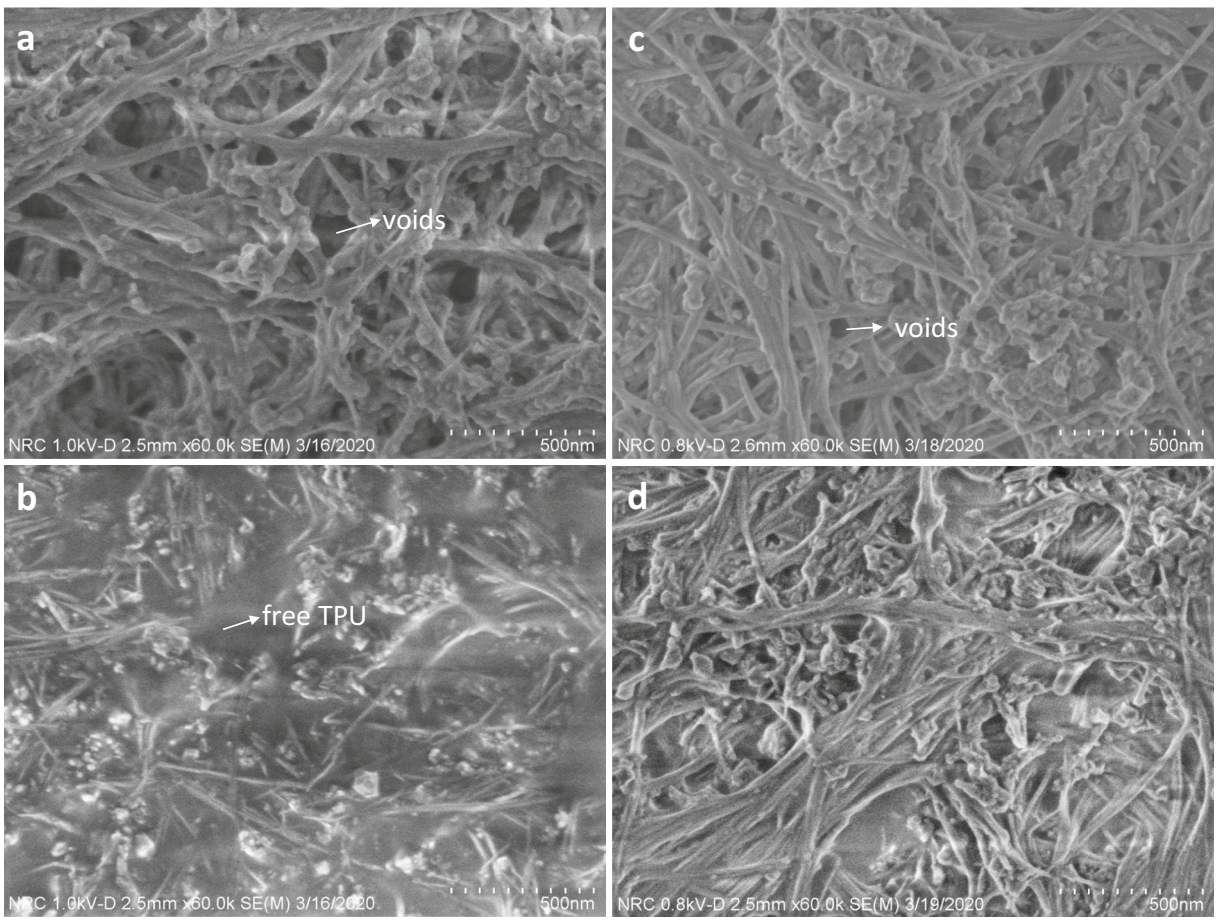

Figure 2: SEM images of the surface of BNNT-TPU composite sheets incorporating BNNT-1 and f-BNNT-2 at different BNNT/TPU weight ratios: (a) BN1-PU-1, (b) BN1-PU-3, (c) f-BN2-PU-1, and (d) f-BN2-PU-3.

nanocomposites also show a fiber-like morphology; however, in contrast to the CNT case, the TPU appears mainly deposited onto BNNT bundles rather than coating individual nanotubes and bundles. This again suggests that the interaction between TPU and BNNT is weaker than that of TPU and CNT.

Controllable tensile properties and nanomechanical mapping

Tensile tests were performed on the nanocomposite sheets to determine the effect of BNNT/TPU weight ratio and BNNT quality on the stiffness, toughness, extensibility, and strength of the nanocomposites. Results for neat TPU are shown in Fig. S5 where three regions commonly observed for pristine TPU are evident: first, the behavior at low deformation and an appearance of a clear yield point; second, the region of plastic flow deformations; and third, the strain hardening region. Figure 3a shows typical tensile stress–strain curves obtained for BNNT-TPU sheets incorporating the f-BNNT-2 material. Table 2 summarizes the tensile mechanical properties of the BNNT-TPU nanocomposite sheets as a function of TPU content. For comparison, nominally 100% BNNT papers (buckypapers) made from BNNTs synthesized and purified by the same methods have Young's modulus ~ 500 MPa, although at lower density (~ 0.3 g/cm^3), but very low strength (~ 2–4 MPa) and failure strain (~ 1%) compared to the BNNT-TPU sheets.

Results indicate up to 12-fold improvement in Young's modulus after the incorporation of BNNTs. A comparison between BNNT-1 and BNNT-2 nanocomposites shows that, despite the similarities in TPU adsorption behavior (Fig. 1), the use of the higher quality BNNT material improved the stiffness of the BNNT-TPU nanocomposites (Fig. 3b). Moreover, the stiffness reaches a maximum at lower BNNT content in the case of f-BNNT and BNNT-2 in comparison with BNNT-1, with BNNT/TPU weight ratios of 49/51 and 42/58 for BNNT-1 and BNNT-2, respectively (indicated by dashed lines in Fig. 3b). The decrease in stiffness above an optimal TPU content was previously understood for CNT-TPU sheets as the result of surpassing an optimal nanotube surface coverage at a critical CNT/TPU weight ratio leading to a combination of adsorbed TPU and free TPU. At the critical nanotube/TPU weight ratio, an optimal nanotube network density/packing and interface contribution (fraction of the polymer phase strongly adhered to the nanotube surface)

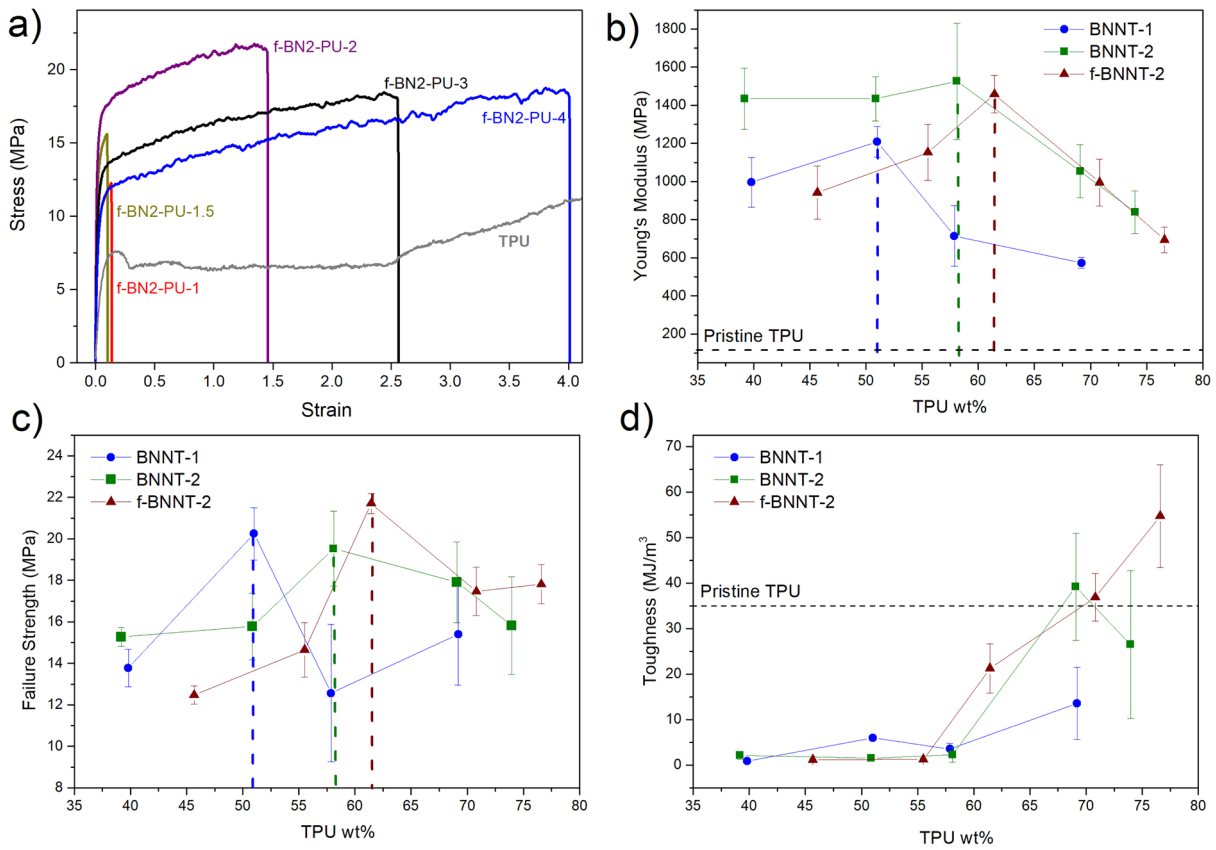

Figure 3: Typical tensile stress–strain curves for BNNT-TPU sheets of different BNNT/TPU weight ratios (Table 1) incorporating functionalized BNNTs (f-BNNT-2) (a). Summary of tensile mechanical properties of nanocomposite sheets incorporating pristine BNNTs of different quality (BNNT-1 and BNNT-2) and functionalized BNNTs (b, c, and d, lines to guide the eye).

TABLE 2: Summary of tensile mechanical properties measured on BNNT-TPU nanocomposite sheets.

Sample	BNNT/TPU weight ratio (w/w)	E (MPa)	σ_{fail} (MPa)	$\sigma_{\varepsilon=30\%}$ (MPa)	ε_{fail} (%)	G_t (MJ/m^3)
BN1-PU-1	60/40	996 ± 130	14 ± 1		7 ± 1	0.9 ± 0.2
BN1-PU-1.5	49/51	1210 ± 80	20 ± 1	20 ± 1	30 ± 2	5.9 ± 0.6
BN1-PU-2	42/58	720 ± 160	12 ± 3	13 ± 3	28 ± 7	4 ± 1
BN1-PU-3	31/69	570 ± 30	15 ± 2	13 ± 2	92 ± 46	14 ± 8
BN2-PU-1	60/40	1440 ± 160	15 ± 0.5		15 ± 6	2.1 ± 0.9
BN2-PU-1.5	49/51	1440 ± 120	16 ± 2		10 ± 3	1.5 ± 0.6
BN2-PU-2	42/58	1500 ± 300	20 ± 2		11 ± 7	2.2 ± 1.6
BN2-PU-3	31/69	1050 ± 140	18 ± 2	15 ± 2	228 ± 80	39 ± 12
BN2-PU-4	26/74	840- ± 110	16 ± 2	13 ± 1	176 ± 81	26 ± 16
f-BN2-PU-1	54/46	940 ± 140	12 ± 0.4		11 ± 2	1.1 ± 0.2
f-BN2-PU-1.5	44/55	1150 ± 150	15 ± 1		9 ± 1	1.2 ± 0.2
f-BN2-PU-2	39/61	1460 ± 98	22 ± 0.5	18.9 ± 0.5	94 ± 24	21 ± 5
f-BN2-PU-3	29/71	990 ± 120	18 ± 1	14.5 ± 0.5	212 ± 28	37 ± 5
f-BN2-PU-4	23/77	690 ± 70	18 ± 1	13.0 ± 0.5	336 ± 64	55 ± 11
TPU	0/100	120 ± 8	34*	5.3 ± 0.3	580*	35*

*From the manufacturer datasheet.

leads to an optimal improvement in the nanocomposite stiffness and strength [25]. In this study, a higher stiffness with a higher TPU content at optimal compositions was observed for the higher quality BNNT-2 material. As disused above and shown in Table 1, an inherent characteristic of the obtained lightweight non-woven sheets is that the void content changes (can be controlled) with the BNNT/TPU ratio and it can also be affected by the network packing. These variations in void content will affect the sheet density and the values of specific modulus, as shown in Fig. S6. However, in a similar way, a higher specific modulus was achieved when BNNT-2 was used. The low specific surface area of low aspect ratio BN impurities still present in the purified BNNT materials was previously demonstrated [28], which likely explains the lower reinforcement observed for BNNT-1 compared to BNNT-2.

It is worth noting that even though a similar TPU adsorption behavior was observed for BNNT-1 and BNNT-2 (Fig. 1), their nanocomposite sheets also showed different adhesion behavior to the membrane filter with a stronger adhesion to the membrane filter observed for BNNT-1 composites as the TPU content increased. This adhesion to the filter limited the recovery of nanocomposite sheets to those with lower TPU contents for BNNT-1 vs BNNT-2 (*i.e.*, BN1-PU-4 cannot be recovered from the membrane filter). Consequently, at equivalent BNNT/TPU weight ratios (*e.g.*, above ~ 50/50 Fig. 3b), the fractions of the polymer phase strongly adhered to the nanotube surface would become lower with increased fractions of unbound or "free" TPU as the TPU content increases. A higher fraction of unbound TPU in BNNT-1 increased the nanocomposite adhesion to the membrane (or any other substrate). This observation is also in agreement with the trend in Young's modulus, which indicates that the optimal surface coverage is achieved at a lower TPU content for BNNT-1 compared to BNNT-2. The results show the importance of BNNT material quality and its effect on composition control affecting not only the tensile mechanical properties but also the adhesion behavior of the TPU nanocomposites.

In addition to the enhanced Young's modulus, the stress in the plastic flow deformation region increases for all nanocomposites. For comparison, the stress at 30% strain (Table 2) shows an increase of up to 4 times at the optimal BNNT/TPU ratio. Trends in failure strength (σ_{fail}) with TPU content are similar to trends in Young's modulus (*i.e.*, higher strength observed at the optimal surface coverage), as shown in Fig. 3d. Noncovalent functionalization with rra-P3HT was not effective to further improve the nanocomposites stiffness over pristine BNNT-2, while the strength was slightly improved at the optimal TPU surface coverage (*i.e.*, f-BNNT-2/TPU weight ratio of 39/61). It is evident from the stress–strain curves that the strain hardening, which is characteristic of TPU, was not observed for the nanocomposite sheets and the failure stress is not improved over the neat TPU regardless of the BNNT material type. This is in contrast with CNT-TPU composites which showed enhancement in failure strength [25].This could result from two effects: (1) a weaker surface interaction between BNNTs and TPU, as proposed above, in comparison with CNTs (for which TPU adsorption was more favorable and improvements in failure tensile strength were achieved); and (2) Morphological changes of TPU in BNNT-TPU composites that prevent soft segments recrystallization to a fiber-like orientation before sample failure.

The modification of the TPU with high contents of the BNNTs decreased the failure strain relative to the TPU matrix

(Table 2), with the lowest quality material (BNNT-1) having a more negative effect. The failure strain generally increases with increasing TPU content once the optimal surface coverage is reached, while the noncovalent functionalization with rra-P3HT can significantly improve the failure strain values. BNNT quality had a significant effect on the tensile properties but most significantly in the failure strain. Low aspect ratio BN impurities with low specific surface area values had less contribution to the interface and probably acted as defect sites and therefore significantly reduced the strain at failure. Consequently, TPU modification on BNNT-2 (pristine and functionalized) offers higher values of absorbed energy before failure (G_t), as shown in Fig. 3d. At equivalent compositions (*e.g.*, BN1-PU-3 and BN2-PU-3), the tensile toughness of nanocomposites incorporating the higher quality BNNT-2 can be three times higher while functionalization (*e.g.*, f-BN2-PU-4 at the 23/77 weight ratio; 14 vol% BNNTs) can lead to further improvements in toughness over pristine BNNT-2 (~ two-fold improvement). Importantly, the increased ductility is achieved with ~ 6- and ~ 2.5-fold improvements in modulus and stress at lower strain (*e.g.*, 30% strain), respectively, in comparison with pristine TPU. The increase in toughness observed for f-BNNT-2 can be attributed to the improved BNNT exfoliation with rra-P3HT functionalization that favored TPU adsorption. This also led to better network packing and BNNT distribution with reduced void fraction as the TPU content increased (Table 1). Additionally, the large increase in toughness could be due to the energy dissipated in disentangling of P3HT alkyl chains [29].

Correlations between sample surface morphology and nanomechanical properties in nanocomposites provide quantitative information on the incorporation and binding interaction between nanomaterials and polymers. Peak Force QNM mode in AFM was conducted on selected BNNT-TPU nanocomposites and pure TPU. Figures 4 and S7 show height images and elastic modulus maps measured on TPU and the nanocomposites. TPUs are linear randomly segmented copolymers consisting of alternating flexible soft segments (SS) and more rigid urethane-containing hard segments (HS). Their unique properties are directly related to their hierarchical morphology and degree of microphase separation. In both the height and elastic modulus maps in Fig. 4a, well-separated phases in the form of ribbon-like hard domains dispersed in the soft segment phase can be clearly observed and the Derjagin-Muller-Toropov (DMT) modulus values can be quantified by the elastic mapping measurements. The distribution of modulus values for the neat TPU was narrow, as previously reported [25], with a peak value of 60 MPa and a shoulder peak at around 30 MPa. AFM images of the BNNT-TPU nanocomposites incorporating the lower quality BNNT-1 material were difficult to image. Different areas showed very different modulus values (Fig. S7a) with significantly higher values observed in areas dominated by BN impurities. Better quality images and elastics maps were obtained for nanocomposites incorporating the higher quality BNNT-2 material at different BNNT/TPU weight ratios (Figs. S7b, 4b and 4c). At lower TPU content (*i.e.*, f-BN2-PU-1 with ~ 50/50 weight ratio), the morphology with tubular structures due to the presence of BNNTs is evident, together with non-tubular BN impurities previously identified in SEM images (Fig. S3). As the TPU content increases above the optimal surface coverage (*e.g.*, f-BN2-PU-3 with ~ 30/70 weight ratio), the microphase segregation of hard segments can be clearly identified, which displays oriented conformation that is normal to the long axis of BNNTs or BNNT bundles (see Fig. S8a for zoom-in images with smaller scan size). Interestingly, the TPU microphase separation observed in BNNT-TPU nanocomposites was not evident in CNT-TPU nanocomposite sheets previously fabricated by the same method [25]. As shown in Fig. S8b, it seems that a homogeneous TPU coating on the CNT surface promotes the mixing of HS and SS domains. Occasionally, in about 10–15% of the areas, we have also observed similar homogeneous TPU coating on the BNNT surface (Fig. S9). These results indicate that a weaker interaction between TPU and BNNTs, combined with the presence of impurities, might lead to more heterogeneous morphologies, thus impacting the nanocomposite mechanical properties.

Thermal conductivity of BNNT fabrics

The thermal conductivities of selected nanocomposite sheets are summarized in Table S1 and Fig. 5 as a function of TPU content. The values of thermal conductivity varied between 1.5 and 3 W m^{-1} K^{-1} (approximately seven to fifteen times more than that of typical polymers), with the highest value obtained for the highest content of unfunctionalized BNNTs. The variation in BNNT quality among the materials did not have a significant effect on thermal conductivity enhancement, which indicates that BN impurities contribute to heat transport similarly to BNNTs within these high BNNT content fabrics, although impurities significantly decreased the sheets' tensile toughness. As expected, the thermal conductivity increases with increased content of BNNT material and the results are comparable to reported BNNT composites with comparably high BNNT content [4, 16]. A simple rule-of-mixtures calculation (see supplementary information) shows that the BNNT-1 and BNNT-2 thermal conductivity results indicate a thermal conductivity of 11–13 W m^{-1} K^{-1} for the BNNT network, slightly higher than estimated from measurements on nominally 100 wt% BNNT paper produced from similar BNNTs [16]. Noncovalent functionalization with a conjugated polymer follows a similar trend to observations for nanocomposite stiffness, showing lower thermal conductivity improvement than with pristine BNNTs above the optimal BNNT/TPU composition and similar thermal conductivities below. For the case of rra-P3HT-functionalized

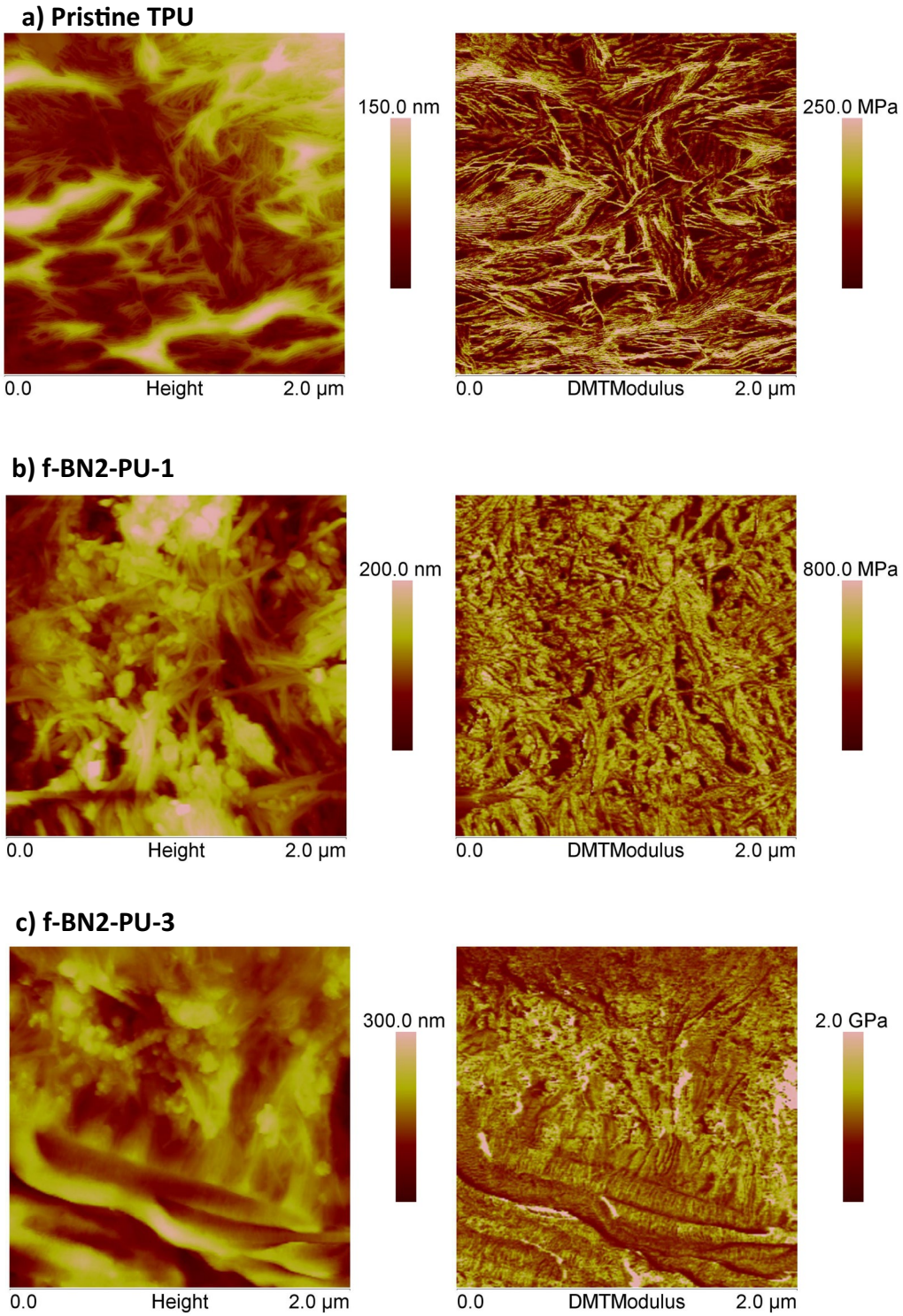

Figure 4: AFM morphology images and elastic modulus maps of TPU (a) and BNNT-TPU nanocomposites with different f-BNNT-2/TPU weight ratios (54/46 for f-BN2-PU-1 (b) and 29/71 for f-BN2-PU-3 (c), respectively). Note that different vertical (z-range) scales were displayed to better visualize the sample morphology and elastic moduli values.

BNNTs, the presence of the conjugated polymer on the BNNT surface reduced the effective thermal conductivity of the BNNT network to ~ 9 W m^{-1} K^{-1} at the highest BNNT content. P3HT has been shown to deposit and align on the BNNT surface [27], and the reduction in thermal conductivity is attributed to increased phonon scattering within the BNNT network at

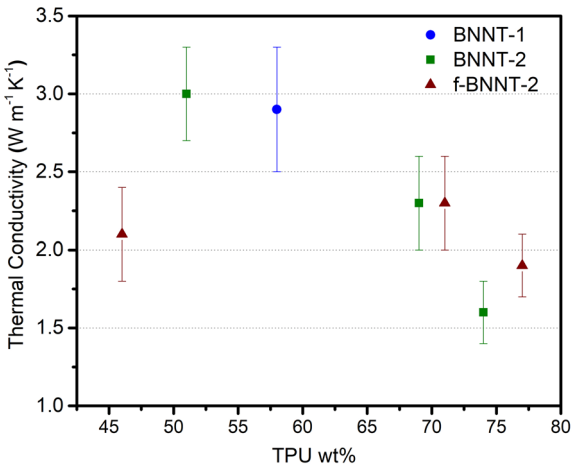

Figure 5: Thermal conductivity of BNNT-TPU nanocomposite sheets prepared by the solvent/non-solvent one-step filtration method using different types BNNT materials.

BNNT-BNNT contacts due to the presence of the rra-P3HT [30]. Unexpectedly, rra-P3HT did not negatively affect the thermal conductivity at lower BNNT content (*i.e.*, ~ 20–30 wt%), which we attribute to a beneficial effect of functionalization on the exfoliation of BNNTs and interaction with TPU above the optimal TPU surface coverage (*i.e.*, at higher TPU content).

Conclusion

Tough, thermally conductive and lightweight BNNT-TPU composite sheets with controlled composition and high content of BNNTs (20–90 wt%) can be fabricated by a one-step filtration process previously applied to the fabrication of CNT-TPU non-woven fabrics. Differences observed in the TPU adsorption behavior to BNNTs in the solvent/non-solvent mixture indicated a weaker interaction between TPU and BNNTs compared to CNTs, requiring an increase of BNNT concentration and of the non-solvent content to enable the recovery of the BNNT-TPU sheets by vacuum filtration. The adsorption behavior was independent of the quality and purity of the BNNT materials evaluated; however, noncovalent functionalization with rra-P3HT appears to improve the surface interactions and favor TPU adsorption on BNNTs. Similar to previous results for CNT-TPU, an optimal surface coverage at a specific BNNT/TPU ratio leads to the highest improvement in Young's modulus and strength and corresponds to the highest fraction of TPU strongly associated with the nanotubes. This specific BNNT/TPU ratio depends on the BNNT quality and shifts to higher TPU content for the higher quality BNNTs (higher specific surface area). Consequently, we expect the adhesive properties of the nanocomposites be different at equivalent BNNT/TPU ratios, which depend on the ratio of free TPU to TPU strongly associated with the nanomaterial. Correlated AFM height images and elastic modulus maps indicated morphological differences depend on the type of nanotube, with CNT promoting hard and soft segment mixing while the microphase segregation of hard segments was clearly identified in the BNNT-TPU composites. The quality of the BNNT material significantly affected the tensile toughness but the effect on thermal conductivity was not evident. Thermal conductivity was determined mainly by BNNT content and reached values of 3 W m^{-1} K^{-1} for the composite sheets with higher BNNT content, roughly 20 times higher than TPU and other typical polymers. The positive effect of rra-P3HT functionalization was mainly observed in the range of BNNT wt% above the optimal surface coverage where incorporation of functionalized BNNTs (f-BNNT-2) showed ~ two-fold improvement in tensile toughness over the unfunctionalized material while maintaining thermal conductivity values (~ 2 W m^{-1} K^{-1}). Importantly, the increased ductility is achieved with ~ 6- and ~ 2.5-fold improvement in modulus and stress at lower strain (*i.e.*, 30% strain), respectively, over pristine TPU. This indicates that the BNNT-TPU nanocomposite could be useful in electronics as a thermally conductive electrical insulator, in particular in combination with its good flexibility and toughness.

Materials and methods

Small diameter (~ 5 nm) BNNTs,were produced in-house by the hydrogen-assisted BNNT synthesis (HABS) process and purified by chlorine etching at 950°C [31, 32]. This gas-phase purification method removes boron impurities and can also remove some BN derivatives, although a significant content of BN impurities can remain in the purified material. BNNT materials from two different synthesis/purification batches namely BNNT-1 and BNNT-2 with BET-specific surface area values of 180 m^2/g and 250 m^2/g, respectively (see supplementary information), were employed in this study. These batches were selected because of the relatively large difference in their surface areas, which were expected to effect the adsorption of TPU in the composite production. The quality of both samples was also analyzed according to a recently reported method based on the adsorption of rra-P3HT on the BNNT surface (Fig. S2) [28], which also shows that the content of impurities is significantly lower for BNNT-2 vs. BNNT-1. The polyurethane was a thermoplastic ester-based polyurethane (UAF 472 by Adhesive Films Inc., Pine Brook, NJ) with density of 1.19 g/cm^3 and a Shore hardness of 85A.

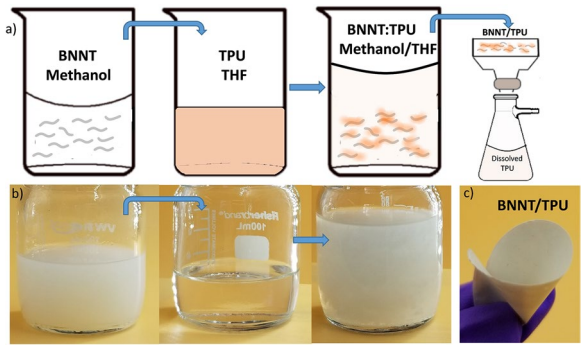

Figure 6: (a) Scheme of the one-step BNNT-TPU sheets fabrication method. (b) Photos of corresponding BNNT suspension, TPU solution, and BNT:TPU suspension in the acetone/methanol mixture prior to vacuum filtration. (c) Photo of a BNNT-TPU nanocomposite sheet.

Fabrication of BNNT-TPU nanocomposite sheets

The one-step filtration method, previously reported for CNTs [25], was adapted to fabricate BNNT-TPU nanocomposite sheets using a suspension of BNNTs dispersed in a TPU solvent/non-solvent mixture. Thirty (30) mg of BNNTs was suspended in 50 mL of methanol using a sonication bath (Fisher Scientific FS110) for 30 min followed by horn sonication (Branson Sonifier 250, 15% output, 50% duty cycle) for 1 min and bath sonication for 30 min. This obtained dispersion settles shortly after the sample is removed from the sonication bath. The BNNT suspension in methanol (Fig. 6) was then added to a TPU solution in THF (30 mL) containing the required amount of TPU to achieve BNNT/TPU weight ratios of 1:1, 1:1.5, 1:2, 1:3, or 1:4 in the solvent mixture (*i.e.*, 50/50, 40/60, 33/67, 25/75, or 20/80 weight ratios in the solvent mixture prior to filtration). The combining of BNNT suspension and TPU solution was facilitated by bath sonication at 20°C for 1 h, followed by horn sonication for 2 min and bath sonication for 30 min. During this step, a fraction of the added TPU is adsorbed on the surface of BNNTs and BNNT bundles. The applied sonication steps are expected to further disentangle BNNT agglomerates and/or bundles, which could be assisted by the polymer chains depending on the interactions between the polymer and BNNTs.

The BNNT:TPU mixtures were filtered, using a Venturi air pump, through a PTFE membrane (1.2 µm pore size). Filtration was completed in 5–10 min. The wet nanocomposite sheets were immediately sandwiched between parchment and filter papers and dried flat at room temperature overnight, after which they were peeled off from the filter membrane, placed between Teflon films, and further dried at 75°C in vacuum for 10 h to remove any residual solvent. The weight fraction of TPU in the final composites was determined by weighing the dried nanocomposites.

For sorption evaluation, the amount of TPU adsorbed per unit mass of BNNTs (C_{ads}) and its remaining concentrations in the solutions (C_{eq}) at equilibrium were determined as follows:

$$C_{ads} = \frac{m_{TPU,comp}}{m_{BNNT}} = \frac{m_{comp} - m_{BNNT}}{m_{BNNT}}, \quad (1)$$

$$C_{eq} = \frac{m_{TPU,sol}}{V_{sol}} = \frac{m_{i,TPU} - m_{TPU,comp}}{V_{sol}}, \quad (2)$$

where m_{BNNT} and $m_{i,TPU}$ are the initial amounts of BNNTs and TPU, respectively, and m_{comp} corresponds to the weight of the dried nanocomposite. $m_{TPU,comp}$, $m_{TPU,sol}$, and V_{sol} correspond to the amount of TPU adsorbed by the BNNTs, the amount of TPU remaining in solution, and the volume (80 mL) of the solution, respectively.

BNNTs functionalized with rra-P3HT were prepared as previously reported [27] by suspending 30 mg of BNNT-2 in 300 mL of $CHCl_3$ with the aid of bath sonication (30 min) and adding, gradually, a solution of rra-P3HT in $CHCl_3$ (0.5 mg/mL). The mixture was bath-sonicated for a total of 50 min. The stable dispersion of rra-P3HT functionalized BNNTs (f-BNNT-2) was then filtered using a Venturi air pump and the wet f-BNNT-2 was immediately re-suspended in 30 mL of methanol before mixing with the TPU dissolved in THF, as described above for unfunctionalized BNNTs.

Characterization

Physical properties of the BNNT-TPU sheets: The external volume of the samples was evaluated by cutting squares of 30 mm by 30 mm from the BNNT-TPU composites. The thickness was measured with a Marathon Digital Electronic Micrometer having a resolution of 0.001 mm. The volume fraction of nanotubes ($V_{f,BNNTs}$), TPU ($V_{f,TPU}$), and pores/voids ($V_{f,voids}$) in the samples were estimated using Eqs. 3, 4, and 5:

$$V_{f,BNNT} = \frac{\rho_{Comp}}{\rho_{BNNT}} W_{f,BNNT,} \quad (3)$$

$$V_{f,TPU} = \frac{\rho_{Comp}}{\rho_{TPU}} W_{f,TPU,} \quad (4)$$

$$V_{f,voids} = 1 - V_{f,TPU} - V_{f,BNNT,} \quad (5)$$

where ρ_{Comp}, ρ_{BNNTs}, and ρ_{TPU} are the nanocomposite sheet, BNNT and TPU densities, respectively. ρ_{Comp} was obtained by dividing the mass of the BNNT-TPU composite sheets by their external volume. The density of the individual BNNTs, 1.9 g/cm^3, was calculated from a geometrical model for nanotubes (see Supplementary information). $W_{f,BNNT}$ and $W_{f,TPU}$ correspond to the weight fraction of BNNT and TPU, respectively, in the BNNT-TPU composite sheets.

Imaging and properties

Scanning electron microscopy (SEM) images were taken with a Hitachi High Technologies S-4800v. Tensile testing was performed using a MTS Criterion C41 Table Top tensile machine with a load capacity of 1 kN. A minimum of five strips (~ 30 mm × 2 mm) of each material were tested at a displacement rate of 5 mm/min and an initial gauge length of ~ 20 mm. Thermal conductivity was measured under vacuum (10^{-5} Torr) at room temperature (300 K) using the parallel thermal conductance (PTC) method [33], and a measurement fixture previously implemented for carbon nanotube yarns [34]. In the PTC method, a BNNT-TPU sheet (5 mm × 12 mm × ~ 0.1 mm) was suspended across a gap between a heater platform and a heat sink. The steady-state thermal conductance (K) was determined through application of a series of known heater powers (P) and plotting the resulting temperature differences (ΔT), where

$$P = K\Delta T. \tag{6}$$

Three measurement results: background thermal conductance (sample removed), total thermal conductance (with sample present), and a radiation correction were used to extract the sample thermal conductance, accounting for sample dimensions, and calculate thermal conductivity [34]. Standard propagation of errors is used to estimate the measurement uncertainty based on the uncertainty in the measured K values and sample dimensions.

Atomic force microscopy (AFM) imaging and elastic modulus mapping were carried out using a MultiMode AFM with the NanoScope V controller (Bruker Nano Surfaces Division, Santa Barbara, CA, USA), in the Peak Force QNM mode. The peak force with which the tip taps the sample surface was always kept at the lowest stable imaging level of 200–400 pN. Silicon nitride ScanAsyst-Air AFM probes (Bruker AFM Probes, Camarillo, CA, USA) were used in all peak force feedback measurements. Their manufacturer-specified typical tip diameter and spring constants are 2 nm and 0.4 N/m, respectively. While images of sizes of up to 20 µm × 20 µm were acquired to ensure good homogeneity nanotube networks, all the images used to measure modulus were 500 nm × 500 nm in size, acquired with 512 × 512 pixel resolution, and the AFM cantilever was vertically oscillated at 2 kHz, at a lateral scan rate of 1 Hz. In this way, the lateral pixel size is approximately 1 nm. The elastic modulus values were analyzed in terms of the distribution of Derjagin–Muller–Toropov (DMT) moduli over the investigated area. In order to obtain reliable results of mechanical properties through AFM, the "relative calibration method" was adopted; details about the "relative method" can be found in the instrument manual provided by Gojzewski et al. [35]. Two reference samples were selected for calibration: polystyrene and polydimethylsiloxane gel with elastic modulus of 2.7 GPa and 3.5 MPa, respectively. The calibration was always carried out before any measurements of the samples characterized.

Acknowledgments

The authors acknowledge the NRC Nanotube Manufacturing Facility (Dean Ruth, Mark Plunkett) for production of the raw BNNT material used in this work. Technical assistance at NRC from Summer Ho, Clement Beausoleil, and Olga Naboka is gratefully acknowledged, as is that from Michel Johnson (Dalhousie University, Canada) for thermal conductivity measurements.

Funding

Open Access provided by National Research Council Canada. Financial support for this work was provided by the Security Materials Technology Program of the National Research Council Canada.

Data availability

All data generated or analyzed during this study are included in this publishing article and supplementary information.

Declarations

Conflict of interest The authors have no conflict of interest to declare.

Supplementary Information

The online version contains supplementary material available at https://doi.org/10.1557/s43578-022-00707-x.

Open Access

References

1. K.S. Kim, M.J. Kim, C. Park, C.C. Fay, S.H. Chu, C.T. Kingston, B. Simard, Scalable manufacturing of boron nitride nanotubes and their assemblies: a review. Semicond. Sci. Technol. **32**, 013003 (2017)
2. R. Arenal, M.S. Wang, Z. Xu, A. Loiseau, D. Golberg, Young modulus, mechanical and electrical properties of isolated individual and bundled single-walled boron nitride nanotubes. Nanotechnology **22**, 265704 (2011)
3. X. Blase, A. Rubio, S.G. Louie, M.L. Cohen, Stability and band gap constancy of boron nitride nanotubes. Euro. Phys. Lett. **28**, 335 (1994)
4. C. Zhi, Y. Bando, T. Terao, C. Tang, H. Kuwahara, D. Golberg, Towards thermoconductive, electrically insulating polymeric composites with boron nitride nanotubes as fillers. Adv. Funct. Mater. **19**, 1857 (2009)
5. Y. Chen, J. Zou, S.J. Campbell, G. Le Caer, Boron nitride nanotubes: pronounced resistance to oxidation. Appl. Phys. Lett. **84**, 2430 (2004)
6. J.H. Kang, G. Sauti, C. Park, V.I. Yamakov, K.E. Wise, S.E. Lowther, C.C. Fay, S.A. Thibeault, R.G. Bryant, Multifunctional electroactive nanocomposites based on piezoelectric boron nitride nanotubes. ACS Nano **9**, 11942 (2015)
7. X.F. Jiang, Q. Weng, X.B. Wang, X. Li, J. Zhang, D. Golberg, Y. Bando, Recent progress on fabrications and applications of boron nitride nanomaterials: a review. J. Mater. Sci. Technol. **31**, 589 (2015)
8. D. Pan, F. Su, H. Liu, Y. Ma, R. Das, Q. Hu, C. Liu, Z. Guo, The properties and preparation methods of different boron nitride nanostructures and applications of related nanocomposites. Chem. Rec. **20**, 1314 (2020)
9. M.B. Jakubinek, B. Ashrafi, Y. Martinez-Rubi, J. Guan, M. Rahmat, K.S. Kim, S. Dénommée, C.T. Kingston, B. Simard, Boron nitride nanotube composites and application, in *Nanotube Superfiber Materials*, 2nd edn., ed. by M.J. Schulz, V. Shanov, Z. Yin, M. Cahay (Elsevier, Amsterdam, 2018), pp.91–111. https://doi.org/10.1016/B978-0-12-812667-7.00005-7
10. C. Tan, Z. Dong, Y. Li, H. Zhao, X. Huang, Z. Zhou, J.W. Jiang, Y.Z. Long, P. Jiang, T.Y. Zhang, B. Sun, A high performance wearable strain sensor with advanced thermal management for motion monitoring. Nat. Commun. **11**, 3530 (2020). https://doi.org/10.1038/s41467-020-17301-6
11. X. Chen, L. Zhang, C. Park, C.C. Fay, X. Wang, C. Ke, Mechanical strength of boron nitride nanotube-polymer interfaces. Appl. Phys. Lett. **107**, 253105 (2015)
12. M. Rahmat, B. Ashrafi, A. Naftel, D. Djokic, Y. Martinez-Rubi, M.B. Jakubinek, B. Simard, Enhanced shear performance of hybrid glass fiber–epoxy laminates modified with boron nitride nanotubes. ACS Appl. Nano Mater. **1**, 2709 (2018)
13. M.B. Jakubinek, B. Ashrafi, Y. Martinez-Rubi, M. Rahmat, M. Yourdkhani, K. Su-Kim, K. Laqua, A. Yousefpour, B. Simard, Nanoreinforced epoxy and adhesive joints incorporating boron nitride nanotubes. Int. J. Adhes. Adhes. **84**, 194 (2018)
14. G. Xiao, J. Di, H. Li, J. Wang, Highly thermally conductive, ductile biomimetic boron nitride/aramid nanofiber composite film. Compos. Sci. Technol. **189**, 108021 (2020)
15. C. Xu, M. Miao, X. Jiang, X. Wang, Thermal conductive composites reinforced via advanced boron nitride Nanomaterials. Compos. Commun. **10**, 103 (2018)
16. M.B. Jakubinek, J.F. Niven, M.B. Johnson, B. Ashrafi, K.S. Kim, B. Simard, M.A. White, Thermal conductivity of bulk boron nitride nanotube sheets and their epoxy-impregnated composites. Phys. Status Solidi A **213**, 2237 (2016)
17. C. Zhi, Y. Bando, T. Terao, C. Tang, H. Kuwaraha, D. Golberg, Towards thermoconductive, electrically insulating polymeric composites with boron nitride nanotubes as fillers. Adv. Funct. Mater. **19**, 1857 (2009)
18. P. Babilo, R. J. Moss, Thermally conductive flexible adhesive for aerospace applications, US9464214B2, The Boeing Company (2016)
19. Y. Shang, G. Yang, F. Su, Y. Feng, Y. Ji, D. Liu, R. Yin, C. Liu, C. Shen, Multilayer polyethylene/ hexagonal boron nitride composites showing high neutron shielding efficiency and thermal conductivity. Compos. Commun. **19**, 147 (2020)
20. Z. Liu, A. Hao, S. Zhang, Y.S. Dessureault, R. Liang, Lightweight carbon nanotube surface thermal shielding for carbon fiber/ bismaleimide composites. Carbon **153**, 320–329 (2019)
21. D. Zhang, K. Cai, J. Pan, L.J. Lee, J.M. Castro, A novel carbon nanotube nanopaper polyurethane coating for fiber reinforced composite substrates. Polym. Eng. Sci. **61**, 1041 (2021)
22. M.B. Jakubinek, Y. Martinez-Rubi, B. Ashrafi, N. Gumienny-Matsuo, D. Park, H. Li, S. Dénommée, B. Simard, Carbon nanotube fabric-based composites for development of multifunctional structures. MRS Adv. **4**(57–58), 3123 (2019)
23. S. Zhang, A. Hao, N. Nguyen, A. Oluwalowo, Z. Liu, Y. Dessureault, J.G. Park, R. Liang, Carbon nanotube/carbon composite fiber with improved strength and electrical conductivity via interface engineering. Carbon **144**, 628–638 (2019)
24. B. Ashrafi, M. Jakubinek, K. Laqua, Y. Martinez-Rubi, B. Simard. Stretchable nanocomposite skin material and related structures. US Patent App. 16/613,878 (2020)
25. Y. Martinez-Rubi, B. Ashrafi, M.B. Jakubinek, S. Zou, K. Laqua, M. Barnes, B. Simard, Fabrication of high content carbon nanotube–polyurethane sheets with tailorable properties. ACS Appl. Mater. Interfaces **9**, 30840 (2017)
26. W. Tan, J.C. Stallard, F.R. Smail, A.M. Boies, N.A. Fleck, The mechanical and electrical properties of direct-spun carbon nanotube mat-epoxy composites. Carbon **150**, 489–504 (2019)
27. Y. Martinez-Rubi, Z.J. Jakubek, M.B. Jakubinek, K.S. Kim, F. Cheng, M. Couillard, C. Kingston, B. Simard, Self-assembly and visualization of poly (3-hexyl-thiophene) chain alignment along boron nitride nanotubes. J. Phys. Chem. C **119**, 26605 (2015)

28. Y. Martinez Rubi, Z.J. Jakubek, M. Chen, S. Zou, B. Simard, Quality assessment of bulk boron nitride nanotubes for advancing research, commercial, and industrial applications. ACS Appl. Nano Mater. **2**, 2054 (2019)
29. T. Sainsbury, A. Satti, P. May, Z. Wang, I. McGovern, Y.K. Gunko, J. Coleman, Oxygen radical functionalization of boron nitride nanosheets. J. Am. Chem. Soc. **134**, 18758 (2012)
30. A. Zandieh, H. Izadi, M. Hamidinejad, H. Shin, S. Shi, Y. Martinez-Rubi, J. Guan, H. Cho, K. Su Kim, C.B. Park, Molecular engineering of the surface of boron nitride nanotubes for manufacture of thermally conductive dielectric polymer composites. Appl. Surf. Sci. **587**, 152779 (2022)
31. K.S. Kim, C.T. Kingston, A. Hrdina, M.B. Jakubinek, J. Guan, M. Plunkett, B. Simard, Hydrogen-catalyzed, pilot-scale production of small-diameter boron nitride nanotubes and their macroscopic assemblies. ACS Nano **8**, 6211 (2014)
32. H. Cho, S. Walker, M. Plunkett, D. Ruth, R. Iannitto, Y. Martinez Rubi, K.S. Kim, C.M. Homenick, A. Brinkmann, M. Couillard, S. Dénommée, J. Guan, M.B. Jakubinek, Z.J. Jakubek, C.T. Kingston, B. Simard, Scalable gas-phase purification of boron nitride nanotubes by selective chlorine etching. Chem. Mater. **32**, 3911 (2020)
33. B.M. Zawilski, R.T. Littleton, T.M. Tritt, Description of the parallel thermal conductance technique for the measurement of the thermal conductivity of small diameter samples. Rev. Sci. Instrum. **72**, 1770 (2001)
34. M.B. Jakubinek, M.B. Johnson, M.A. White, C. Jayasinghe, G. Li, W. Cho, M.J. Schulz, V. Shanov, Thermal and electrical conductivity of array-spun multi-walled carbon nanotube yarns. Carbon **50**, 244 (2012)
35. H. Gojzewski, B. Imre, C. Check, R. Chartoff, J. Vancso, Mechanical mapping and morphology across the length scales unveil structure-property relationships in polycaprolactone based polyurethanes. J. Polym. Sci. Part B Polym. Phys. **54**, 2298 (2016)